Chapter 8
Anhydrite Formation on the Coastal Sabkha of Abu Dhabi, United Arab Emirates

Michael A. Wilson, Shabbir A. Shahid, Mahmoud A. Abdelfattah, John A. Kelley, and James E. Thomas

Abstract A fluvial marine sabkha along the coastal area of Abu Dhabi, United Arab Emirates, is hypersaline from evaporative losses of groundwater originating from rain, seawater intrusion, lagoons that border the sabkha, and inland groundwater sources. Anhydrite ($CaSO_4$) is present in these soils and is regarded to be both a neoformed mineral and a product of gypsum transformation. Six pedons (designated 1–6) were described, sampled, and characterized from a 13-km transect across the sabkha in order to better understand the distribution of anhydrite across the sabkha, determine suitable laboratory methods for detection and quantification of this mineral, and evaluate soil genesis and mineral formation. Soils were highly saline

M.A. Wilson (✉)
United States Department of Agriculture-Natural Resources Conservation Service, National Soil Survey Center, 100 Centennial Mall North, Rm 152, Lincoln, NE 68508–3866, USA
e-mail: mike.wilson@lin.usda.gov

S.A. Shahid
International Center for Biosaline Agriculture, P.O. Box 14660, Dubai, UAE
e-mail: s.shahid@biosaline.org.ae

M.A. Abdelfattah
Soil and Land Use Management, Environment Agency-Abu Dhabi, P.O. Box 45553, Abu Dhabi, UAE

Soils and Water Sciences Department, Faculty of Agriculture, Fayoum University, Fayoum, Egypt
e-mail: mabdelfattah@ead.ae; mahmoudalia@yahoo.com

J.A. Kelley
United States Department of Agriculture-Natural Resources Conservation Service, Raleigh, NC, USA
e-mail: bettmark.john@gmail.com

J.E. Thomas
United States Department of Agriculture-Natural Resources Conservation Service, National Soil Survey Center, 100 Centennial Mall North, Rm 152, Lincoln, NE 68508-3866, USA

S.A. Shahid et al. (eds.), *Developments in Soil Classification, Land Use Planning and Policy Implications: Innovative Thinking of Soil Inventory for Land Use Planning and Management of Land Resources*, DOI 10.1007/978-94-007-5332-7_8,

with electrical conductivity (EC1:2) ranging from 11 to 167 dS m^{-1}. Evaporative minerals identified by x-ray diffraction include calcite, gypsum, halite, aragonite, and anhydrite. Together, salts, gypsum, and anhydrite composed 5–100% of the mineral matter of sabkha soils. Quantification of anhydrite was achieved by the difference in the acetone method (gypsum + anhydrite quantification) and low-temperature weight loss (for gypsum quantification). Both a thermal gravimetric analyzer (TGA) and an oven were tested for the latter procedure. The TGA method was found to provide the most reliable data, while the oven method yielded inconsistent results. Anhydrite was identified in the two sites (pedons 5 and 6) most distant from the coast, ranging up to 43% of the <2-mm fraction and occurring in thicknesses of 70 and 55 cm, respectively.

Keywords Fluvial marine • Anhydrite formation • Coastal sabkha • Hypersaline • Evaporative • Abu Dhabi • Thermal analysis

8.1 Introduction

Sabkhas (salt flats) are widely distributed in the coastal areas around the world. Detrital sediments, plus soluble elements from the marine environment, create a suite of carbonate, chloride, and sulfate minerals. The climate of the Arabian Peninsula creates unique conditions that influence the resulting mineralogical suite in sabkhas of this area. Anhydrite ($CaSO_4$) is a mineral that has been documented in this area, both a neoformed mineral and as a product of gypsum ($CaSO_4 \cdot 2H_2O$) transformation, due to the combined effects of high salinity and temperature. Anhydrite develops in these soils and remains stable in the vadose zone above the water tables (Aref et al. 1997; Sanford and Wood 2001; El-Tabakh et al. 2004; Shahid et al. 2007). This process is well documented to occur during carbonate deposition where anhydrite is a common by-product (along with gypsum) associated with seawater evaporation (El-Tabakh et al. 2004; Melim and Scholle 2002). Often this process occurs under elevated burial temperatures or due to hot fluid-rock interactions (Kasprzyk and Orti 1998).

The coastal area of Abu Dhabi, United Arab Emirates (UAE), is hypersaline from evaporative losses of groundwater originating from rain, seawater intrusion, lagoons that border the sabkha, and inland groundwater sources. Sanford and Wood (2001) documented that the water within the sabkha soils of Abu Dhabi is principally derived from rainfall, with the major source of solutes from the slowly permeable Tertiary formations of marl and gypsum that underlie the sabkha and create episaturated conditions within soils. Their results show that the lateral intrusion of seawater is very low due to the slow groundwater flux due principally to the low gradient of the sabkha (typically 2×10^{-4} m m^{-1}) (Sanford and Wood 2001).

The recent soil survey of the Abu Dhabi Emirate (EAD 2009) has documented the presence of mapping units principally composed of soils dominated by anhydrite within the coastal sabkha. This discovery resulted in a formal proposal for the

modification of Soil Taxonomy (Soil Survey Staff 2010). This proposal included the formation of an anhydritic family mineralogy class to separate these soils dominated by anhydrite from gypsum-rich soils (Abdelfattah and Shahid 2007; Shahid et al. 2007). The inclusion of this family mineralogy class in Soil Taxonomy requires the quantification of anhydrite. This study was created to help determine the distribution of this mineral in the broad, level mapping units of Abu Dhabi sabkhas and to investigate laboratory methods that would assist in the identification and quantification of anhydrite. Thus, the objectives of this study are to investigate methods to identify and/or quantify anhydrite in soils, determine the distribution of anhydrite in selected soils across a coastal sabkha, and discuss factors affecting the genesis and distribution of this mineral. Knowledge gained in this study should have applicability across the region, but also globally in other arid, hot coastal and inland regions (e.g., playas) that are locations of salt accumulations.

8.2 Materials and Methods

8.2.1 Soil-Forming Factors

Abu Dhabi is located on the north coast of the Arabian Peninsula within the United Arab Emirates (Fig. 8.1). The coastal area of Abu Dhabi is composed of three geomorphic areas: islands, shoal and channel areas of the lagoons, and the coastal sabkha (Butler 1970). The fluvial marine sabkha (broad coastal plain) is over 400 km in length and up to 16 km in width (de Matos 1989). The sabkha slopes toward the sea at about 0.4 m km^{-1} (Evans et al. 1969). Tertiary-aged geologic materials underlie and border the sabkha on the southeastern perimeter, partially buried at the surface by Holocene-aged dunes and gravels. The sabkha is composed of Quaternary (Pleistocene and Holocene-aged) sediments derived from aeolian and fluvial materials, with overlying lagoon and tidal deposits, and other evaporative and chemically precipitated minerals developed in this current environment (Evans et al. 1969; Butler 1970). The water table forms by water perching on the Tertiary-aged strata that underlie the sands (Sanford and Wood 2001).

The aeolian sediments were principally deposited during a stage when the Arabian Gulf was dry and winds transported the exposed sands from the gulf bottom onto the land area along the coast (Alsharhan and Kendall 2003). The sand is currently about 10 m deep (Sanford and Wood 2001). Following the last glacial maximum (18,000 years before present-ybp), water transgressed and reached the present shoreline by 6,000 ybp (Lambeck 1996). The maximum transgression of the sea inundated the area for a short time following this period, then regressed to its present level when the current shoreline was established (Evans et al. 1969). The area has been relatively stable and undergoing pedogenic development for about 4,000–5,000 years (Evans et al. 1969; Lambeck 1996).

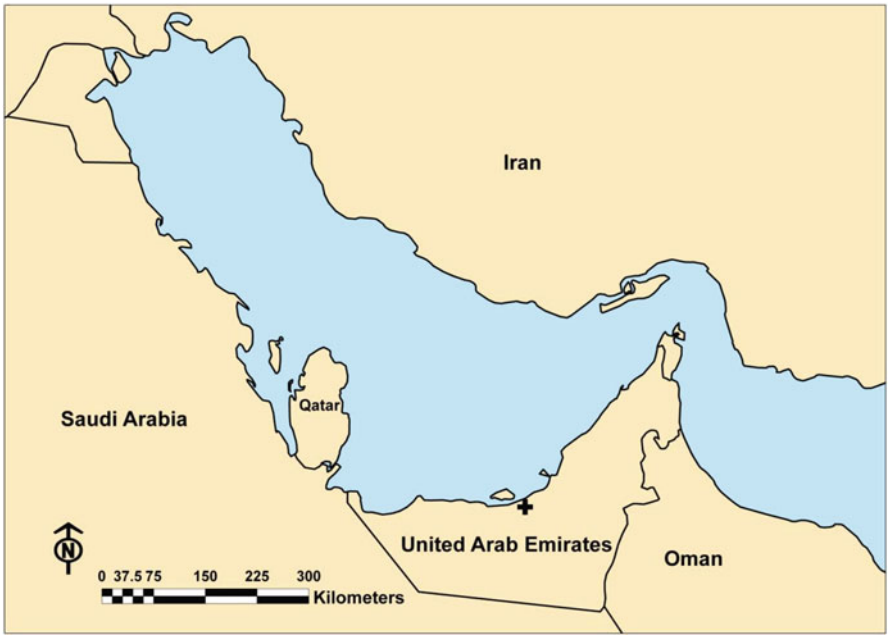

Fig. 8.1 Map showing the location of the United Arab Emirates. The "x" denotes to general area of the study

8.2.1.1 Climate

Summer temperatures are extremely hot (mean summer temperature of 32.8°C) with maximum temperatures between June and September, ranging up to and exceeding 50 °C. Winters (December to February) are characterized as short and mild, with a mean temperature of 19.0 °C (minimum temperature as low as 3°C). Mean annual rainfall is 29 mm (NCMS 2009). Vegetation is largely absent in the sabkha but includes blue-green algal mats in intertidal zones and sparsely populated halophytes.

8.3 Sampling and Laboratory Analysis

A 13-km-long transect was established across the sabkha starting at the shoreline (Fig. 8.2). Six pedons were sampled by horizon and macromorphology described (Schoeneberger et al. 2002). Bulk samples were air dried and sieved to <2-mm. Laboratory analyses followed by codes were performed according to Burt (2004). For particle size distribution analysis (PSDA) (method 3A1), the fine-earth fraction was dispersed following removal of organic matter and soluble salts, and the sand fraction was separated by wet sieving. Silt and clay fractions were measured by pipette method. Total C, N, and S was determined by dry combustion (6A2f) and

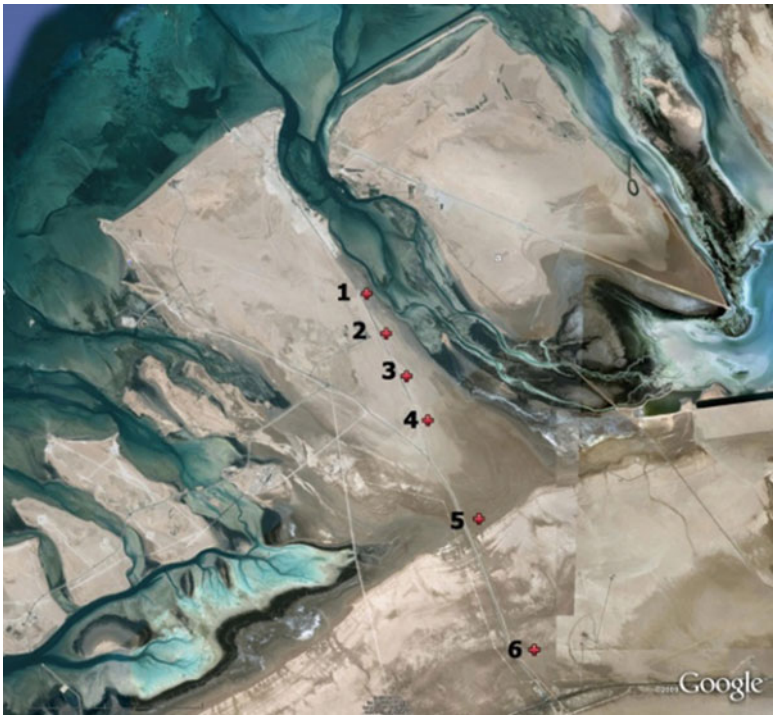

Fig. 8.2 Study area showing the six sites. Distance from site 1 to site 6 is 13 km

calcium carbonate equivalent (CCE) by use of an electronic manometer to quantify gas evolution following acid contact in a closed vessel (6E1g). Total analysis of the <2-mm fraction was determined by microwave digestion in concentrated HF, HNO_3, and HCl, with determination of elements by ICP spectroscopy (4H1b). Electrical conductivity (EC1:2) was measured on a 1:2 (soil to solution) mixture (4F1a1a1). The liquid from a saturated paste was extracted and electrical conductivity (ECsat), cations, and anions determined (4F2). The equivalent gypsum content (EGC) was measured using the method of Elrashidi et al. (2007). Intact pieces of soil fabric were collected and dipped in an elastic saran mixture, with bulk density (4A1d) and water retention (4B1c) quantified at 33 kPa. Water retention at 1,500 kPa was measured on <2-mm air-dried soil (3C2a1a).

Anhydrite was quantified by the difference in two measurements: (a) water dissolution/acetone precipitation (4E2a) that measures both gypsum and anhydrite and (b) gypsum by weight loss. Measurement of gypsum by quantifying the weight of the crystalline waters of hydration was determined by using both thermal gravimetric analysis (TGA) and the method of Artieda et al. (2006). The TGA method measured the weight loss by heating the sample from 20 to 200 °C at a rate of 2 °C min^{-1}. The weight of water loss between 75 and 115°C was used to quantify the gypsum based on a theoretical weigh loss of 20.9% (Karathanasis and Harris 1994).

The Artieda method measured the weight loss of a sample between the temperatures of 70 and 90°C, and gypsum was calculated by

$$\begin{aligned}\text{Percent Gypsum} &= \left\{\left[\left(\text{ws}-\text{wf}\right)/\left(\text{ws}-\text{wt}\right)\right]100\left[\left(100/14.95\right)\right]\right\} \\ &= \left[\left(\text{ws}-\text{wf}\right)/\left(\text{ws}-\text{wt}\right)\right]669\end{aligned} \tag{8.1}$$

with

ws = weight of sample dried at 70 ºC plus weight of sampling dish
wf = weight of sample dried at 90 ºC plus sampling dish
wt = weight of sampling dish
14.95 = the recovery factor of gypsum between 70 and 90 °C

A Pyrex crystallizing dish was used for drying the sample. Weights were collected for several days at multiple temperatures. Based on agreement with both a gypsum mineral standard plus laboratory soil standard with gypsum quantified by the acetone method, reported data was recorded at both 70 and 90 °C after 3 days of equilibration in the oven at the respective temperature.

Mineralogy of the <2-mm fraction was performed by crushing the soil material to less than 0.02 mm, placing on a deep-well slide holder, and analyzing by Cu-K alpha radiation from 2 to 60°2Θ. The mineral composition of the fine sand (0.1–0.25 mm) or very fine sand (0.05–0.1 mm) fraction (following particle size analysis procedure that removes salts and gypsum) was determined by mounting the grains on a glass slide with an epoxy cement (refractive index = 1.54) and counting 300 grains using a petrographic microscope with plane- and cross polarized light (7B1a2). Thin sections of intact soil material were prepared by epoxy impregnation (refractive index = 1.54). The soil fabric was examined with a polarizing petrographic microscope and features described.

8.4 Results

8.4.1 Field Morphology

All pedons were weakly developed and commonly light yellowish or pale brown at the surface (10YR 6/4 or 6/3) to white or light gray (10YR 8/1 or 7/2) in the subsoil (Table 8.1). The soils are generally sandy textured. White or light gray carbonate or gypsic cemented layers were present in the subsoil of most pedons. Sanford and Wood (2001) described similar features as algal and dolomitic crusts. Small seashells were found in the subsoil (generally at depths between 50 and 100 cm) of pedons 3, 4, and 5, suggesting that these layers were developed when the area was submerged in water. The depth to the water table at time of sampling ranged from 105 to 130 cm in all soils with the exception of the tidally influenced pedon nearest the seashore. Thin, cemented surface crusts were present at most sites.

Table 8.1 Selected physical properties of the soils

Horizon	Depth (cm)	Field texture	Moist color[a]	Clay	Silt	Sand	Bulk density 33 kPa	Water retention 33 kPa	Water retention 1,500 kPa
				(%)			(g cm^{-3})	(%)	
Sabkha site 1									
Cz1	0–3	Fine sand	2.5Y 6/3	5.2	14.6	80.2	1.40	11.6	3.8
Cz2	3–7	Coarse sand	2.5Y 7/3	5.6	9.6	84.8	1.66	11.6	3.9
Cz3	7–16	Sand	2.5Y 6/3	1.9	5.6	92.5	1.65	5.1	2.7
Cz4	16–42	Sand	2.5Y 6/3	1.6	0.1	98.3	1.65	3.8	2.0
R	42–46	Cemented		2.8	11.8	85.4			1.4
Sabkha site 2									
Salt crust	–	–	–	4.6	11.4	84.0	–	–	3.3
Az1	0–10	Sand	10YR 7/4	5.2	19.2	75.6	–	–	4.4
Az2	10–20	Sand	10YR 8/3	8.7	12.6	78.7	1.24	17.8	7.3
Bkz1	20–42	Sand	10YR 8/1	7.2	7.3	85.5	1.25	16.1	7.2
Bkz2	42–68	Sand	2.5Y 8/2	6.4	7.4	86.2	1.60	16.6	5.2
Bkzm	68–92	Cemented	2.5Y 5/3	3.4	13.2	83.4	1.78	6.0	3.3
Byz	92–107	Sand	5Y 4/2	1.6	6.2	92.2	1.65	6.8	2.2
Cyzg	107–150	Sand	5Y 5/1	1.9	4.3	93.8	–	–	1.5
Sabkha site 3									
Salt crust	–	–	–	5.4	12.3	82.3	–	–	2.9
Az	0–8	Sand	2.5Y 7/2	9.3	21.9	68.8	1.37	23.8	4.1
Bkyz	8–22	Loam	5Y 8/1	15.9	15.7	68.4	1.18	34.1	7.5
Bkyz	22–38	Sand	2.5Y 7/3	5.2	4.5	90.3	1.29	16.4	3.5
Bkyzm	38–56	Cemented	2.5Y 7/3	2.6	3.2	94.2	1.69	15.6	2.5
B'kyz	56–59	Coarse sand	2.5Y 7/3	2.1	2.8	95.1	1.48	13.5	2.6
B'kyzm	59–70	Cemented	2.5Y 7/3	1.4	4.6	94.0	1.45	10.6	2.1
BCkyz	70–105	Sand	2.5Y 6/2	0.9	1.8	97.3	1.70	6.3	2.3
Ckyzg	105–150	Sand	5Y 5/1	1.8	2.1	96.1	1.62	8.8	2.5

(continued)

Table 8.1 (continued)

Horizon	Depth (cm)	Field texture	Moist color[a]	Clay	Silt	Sand	Bulk density 33 kPa	Water retention 33 kPa	Water retention 1,500 kPa
				(%)			(g cm^{-3})	(%)	
Sabkha site 4									
Salt crust	–	–	–	3.0	11.9	85.1	–	–	3.4
Az	0–7	Sand	2.5Y 6/3	3.2	14.7	82.1	1.51	13.7	5.0
Bkyz	7–20	Sand	2.5Y 6/3	0.7	4.5	94.8	1.50	13.9	4.5
Bkyzm	20–23	Cemented	2.5Y 6/2	2.0	5.2	92.8	1.62	15.0	3.5
B'kyz1	23–60	Sand	2.5Y 6/2	3.1	6.8	90.1	1.46	11.7	4.9
B'kyz2	60–90	Fine sandy loam	5Y 8/1	9.8	8.5	81.7	1.43	19.3	6.2
B'kyz3	90–115	Loam	5Y 8/2	14.2	11.5	74.3	1.29	24.8	9.0
BCkyz	115–123	Loamy sand	2.5Y 6/2	5.7	4.9	89.4	1.31	15.5	4.3
Cyzg	123–150	Sand	5Y 6/1	8.4	15.3	76.3	1.19	20.0	5.5
Sabkha site 5									
Akyz1	0–10	–	10YR 6/4	3.9	10.7	85.4	1.53	16.8	4.1
Bkyz	10–27	Sand	2.5Y 5/3	4.8	16.5	78.7	1.44	15.7	7.5
Bz	27–35	Clay	10YR 8/1	10.0	52.2	37.8	0.98	56.2	5.4
Bkyz1	35–50	Sand	10YR 7/2	5.3	21.1	73.6	1.23	27.5	14.4
Bkyz2	50–70	Sand	Gley 1 8/10Y	16.6	34.2	49.2	1.14	28.1	12.0
2Bk1z1	70–95	Sand	Gley 1 7/10Y	10.2	15.8	74.0	1.10	31.7	7.6
2Bk2z2	95–110	Sand	Gley 1 7/10Y	5.0	11.7	83.3			4.1
Sabkha site 6									
Akz	0–5	Sand	10YR 6/3	7.2	23.1	69.7	1.31	23.0	3.1
Bz	5–40	Clay	10YR 8/1	8.4	81.4	10.2	0.96	49.3	4.1
Bkyz	40–50	–	Gley 1 7/N	5.1	62.7	32.2	1.12	42.0	24.4
Byzm	50–55	Cemented	10YR 8/1	3.0	40.0	57.0	1.65	13.5	1.7
Ck1z1	55–100	Sand	2.5Y 5/4	1.8	1.6	96.6	1.60	4.2	1.4
Ck2z2	100–140		2.5Y 5/3	2.7	1.2	96.1	1.62	4.4	1.6

[a] Munsell color notation

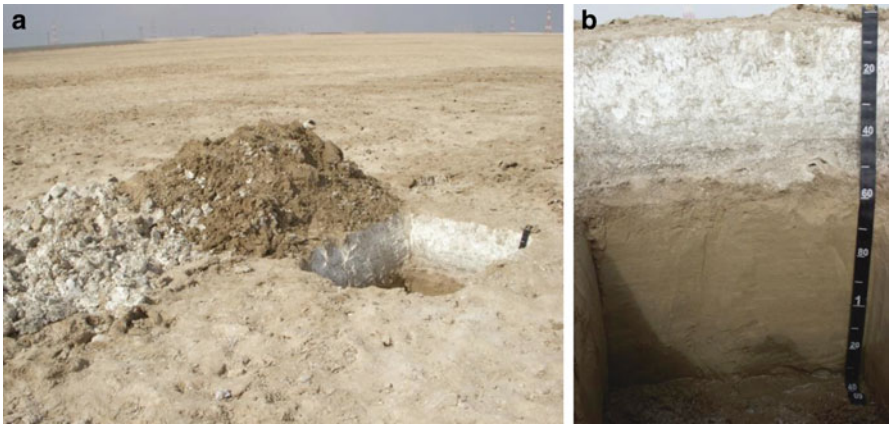

Fig. 8.3 Landscape (**a**) and profile of pedon 6 (**b**). Anhydrite is the *white zone* in the *upper part* of the profile

Specific morphological indicators were regarded by the authors as unique to mineral concentrations of anhydrite in this environment. They were a combination of white color (5Y or 10YR 8/1 or 8/2), clayey/silty textures, and/or thixotropic nature. Based on these field criteria, the Bkyz horizon (8–22 cm) of pedon 3, B'kyz2 (60–90 cm) and B'kyz3 horizons (90–115 cm) of pedon 4, Bz horizon (27–35 cm) of pedon 5 (Fig. 8.3a, b), and Bz (5–40 cm) and Bkyz (40–50 cm) of pedon 6 were regarded as possible layers with accumulations of anhydrite.

8.4.2 Carbonates, Equivalent Gypsum, and Salts

Pedon 1, the site closest to the shoreline, has the lowest salt concentrations of all sampled pedons with EC1:2 ranging from 10.7 to 23.7 dS m^{-1} (Table 8.2). The site is tidally influenced (component of the intertidal zone) and any salts that precipitate by evaporation would be transient with diurnal fluctuation of the water. The pH is highest in this pedon (8.5–8.9) relative to the other sites in the study.

The other pedons (2–6) have salt accumulation in surface horizons, with EC1:2 values (Table 8.2) ranging from 84 to 162 dS m^{-1}. The ECsat on some surface horizons exceeded the detection limits of the instrument (>200 dS m^{-1}). The EC1:2 in subsoil horizons varies from 29 to 95 dS m^{-1} (ECsat = 90–190 dS m^{-1}). Saturated paste EC values are higher than EC1:2 due to lower dilution ratios and provide a reasonable measure of soluble salt concentrations present in solution at field capacity, though all salts are not dissolved at this water content. The EC1:2 is advantageous as this value represents a fixed soil to water ratio, resulting in more comparable salinity values between horizons.

Equivalent gypsum content is a good measure of total water soluble minerals (gypsum, anhydrite, and minerals more soluble) of the <2-mm soil material.

Table 8.2 Selected chemical properties of the soils

Horizon	Depth (cm)	EC (1:2) (dS m^{-1})	EC (sat)	Equiv. gypsum %	$CaCO_3$	$\Sigma EqGy+CaCO_3$	pH
Sabkha site 1							
Cz1	0–3	16.5	86.2	29	47	76	8.7
Cz2	3–7	10.7	53.4	33	48	81	8.5
Cz3	7–16	13.5	74.0	6	61	67	8.5
Cz4	16–42	23.7	113.7	7	67	74	8.7
R	42–46	19.5			84		8.9
Sabkha site 2							
Salt crust		129.9	>200	67	44	111	7.6
Az1	0–10	140.1	>200	66	42	108	7.6
Az2	10–20	55.3	186.4	23	69	92	8.1
Bkz1	20–42	48.1	151.6	18	82	100	8.5
Bkz2	42–68	48.4	167.1	15	80	95	8.3
Bkzm	68–92	36.1	123.6		74		8.1
Byz	92–107	46.7	141.1	16	63	79	8.0
Cyzg	107–150	40.0	148.5	11	61	72	7.9
Sabkha site 3							
Salt crust		167.4	>200	76	44	120	7.5
Az	0–8	130.1	>200	62	52	114	7.7
Bkyz	8–22	65.6	175.4	23	77	100	7.9
Bkyz	22–38	38.5	119.4	15	87	102	8.3
Bkyzm	38–56	38.1	110.1	16	87	103	8.1
B'kyz	56–59	29.6	89.6	12	89	101	8.2
B'kyzm	59–70	41.8	119.7	16	82	98	8.1
BCkyz	70–105	45.4	141.2	17	81	98	8.2
Ckyzg	105–150	55.0	176.1	19	73	92	7.9
Sabkha site 4							
Salt crust		147.6	>200	68	42	110	7.2
Az	0–7	83.7	>200	34	45	79	7.7
Bkyz	7–20	29.4	103.6	10	55	65	7.9
Bkyzm	20–23	31.5	97.2	31	47	78	7.9
B'kyz1	23–60	38.2	115.3	18	57	75	7.6
B'kyz2	60–90	48.7	146.8	16	77	93	7.7
B'kyz3	90–115	65.1	146.1	24	81	105	7.8
BCkyz	115–123	50.3	151.0	18	84	102	7.9
Cyzg	123–150	67.8	151.6	22	73	95	7.6
Sabkha site 5							
Akyz1	0–10	135.1	>200	75	39	114	7.4
Bkyz	10–27	30.8	147.0	38	44	82	7.8
Bz	27–35	91.4	190.3	95	14		7.6
Bkyz1	35–50	47.5	175.0	76	30	106	7.9
Bkyz2	50–70	49.3	164.1	56	48	104	7.9
2Bk1z1	70–95	74.4	181.3	25	72	97	8.0

(continued)

Table 8.2 (continued)

Horizon	Depth (cm)	EC (1:2) (dS m^{-1})	EC (sat)	Equiv. gypsum %	$CaCO_3$	$\Sigma EqGy+CaCO_3$	pH
2Bk2z2	95–110	57.1	162.7	26	80	106	8.1
Sabkha site 6							
Akz	0–5	161.9	>200	98	26	124	7.5
Bz	5–40	95.9	129.9	108	4	112	7.7
Bkyz	40–50	52.9	104.5	71	35	106	8.1
Byzm	50–55	47.3	171.0		6		7.9
Ck1z1	55–100	29.0	155.1	9	34	43	8.3
Ck2z2	100–140	31.7	140.5	11	28	39	8.2

These EGC values (Table 8.2) ranged from 34 to 98% in pedons 2–6. Equivalent gypsum generally decreased in the subsoil and was <25% in the subsoil of all pedons. Carbonates were generally the lowest in the surface where they ranged from 26 to 52% and up to 89% in the subsoil. Together, these two mineral groups (as measured by EGC and CCE) composed from 70 to 100% of the mineral matter in most horizons. The salt crusts sampled for pedons 2, 3, and 4 were composed of about 40% carbonates and 60% equivalent gypsum materials. For two of the three pedons, the equivalent gypsum is only slightly higher in the salt crust than in the A horizon (which included the salt crust). These results suggest that the "salt crust" is similar in composition to the surface soil horizon in these sites.

Elemental analysis of saturated paste extracts (Table 8.3) shows that Na >> Mg > Ca > K. Sodium had the highest concentration due to the greater solubility of Na salts in the saturated paste compared to other minerals. This was reflected in sodium adsorption ratio (SAR) values exceeding 300 in certain horizons. Magnesium is between 2 and 3 times higher in concentration in saturated paste extracts relative to Ca. Suarez (2005) indicates a ratio of Mg/Ca in seawater of 5, similar to these results. Mg is commonly higher due to the lower solubility of Ca minerals such as calcite, aragonite, and gypsum, thus creating a sink for the Ca ions in solution. Total analysis of the <2-mm fraction (Table 8.3) indicated a much greater abundance of Ca overall, with a Ca to Na ratio ranging from 1:1 to 28:1 and an average of 10:1. This ratio is similar for Mg, with an average Ca to Mg ratio of 11:1. These results illustrate an overall greater abundance of Ca in the soil matrix.

Chloride was the dominant anion in saturated paste extracts, generally 30–60 times higher than SO_4. Carbonate anions were not present; bicarbonate was <1 mmol L^{-1}. This ratio decreased in horizons associated with anhydrite formation ranging from 10 to 35%, reflecting an increase in SO_4 content of these horizons. This increase in S is also reflected in the total S, ranging up to 16%S.

8.4.3 Measurements for Gypsum and Anhydrite

The acetone measurement cannot differentiate between gypsum and anhydrite and extracts both minerals together. The results (Table 8.4) show that minerals in this

Table 8.3 Elemental data from saturated paste extracts and total analysis

		Saturated paste							Total elemental analysis						
	Depth	Ca	Mg	Na	K	Cl	SO_4		Si	Al	Ca	Mg	Mn	Na	S
Horizon	(cm)	(mmol L^{-1})						SAR	(mg kg^{-1})						(%)
Sabkha site 1															
Cz1	0–3	51.7	232.0	777.6	20.6	1021.6	176.9	65	92,953	14,775	210,547	33,805	263	11,812	3.06
Cz2	3–7	47.8	122.5	433.6	12.6	536.2	120.4	47	70,897	11,063	227,988	35,762	215	8,134	4.33
Cz3	7–16	57.6	129.0	660.4	17.6	825.9	114.9	68	99,565	15,251	240,036	20,514	227	15,733	0.18
Cz4	16–42	54.9	270.0	1245.0	32.4	1513.6	137.9	98	114,458	17,822	226,107	25,199	284	13,213	0.07
R	42–46								43,963	5,707	320,107	9,155	105	10,518	0.07
Sabkha site 2															
Salt crust		158.6	304.0	5030.0	83.8	5418.5	47.3	331	114,838	12,552	176,108	42,766	307	46,712	1.65
Az1	0–10	186.8	578.0	4468.0	124.0	5402.1	36.4	228	55,586	8,777	184,178	18,593	185	104,935	0.95
Az2	10–20	131.9	309.0	2733.0	63.0	3259.0	75.4	184	40,820	6,748	279,683	20,719	124	28,896	0.76
Bkz1	20–42	87.0	264.0	1882.5	45.5	2281.7	42.2	142	71,512	10,157	134,704	22,950	199	115,744	0.14
Bkz2	42–68	100.2	322.0	2204.5	64.5	2736.4	49.0	152	30,322	3,837	311,350	14,352	77	24,053	0.16
Bkzm	68–92	120.9	193.0	1609.0	40.6	1849.2	98.5		41,361	4,629	307,514	14,098	81	29,462	0.70
Byz	92–107	107.3	253.0	1913.0	52.2	2286.0	78.5	143	74,250	8,616	258,980	20,206	125	32,336	0.27
Cyzg	107–150	108.5	274.0	2004.0	59.8	2509.2	76.8	145	61,601	8,376	170,842	15,524	185	127,318	0.22
Sabkha site 3															
Salt crust		144.0	303.0	5184.0	43.6	5699.1	45.2	347	79,850	12,341	216,292	32,677	176	16,236	1.34
Az	0–8	145.4	337.0	4801.0	62.4	5436.3	49.4	309	117,363	14,594	183,164	37,060	268	8,622	1.45
Bkyz	8–22	127.4	239.0	2936.0	71.8	3289.3	56.2	217	66,988	9,436	183,766	23,728	172	5,889	0.16
Bkyz	22–38	77.4	167.0	1495.0	37.0	1791.2	39.6	135	88,428	9,425	198,334	25,335	161	7,241	0.22
Bkyzm	38–56	114.4	200.0	1298.0	35.0	1594.7	86.1	104	54,256	7,777	291,112	16,258	130	24,052	0.42
B'kyz	56–59	105.3	275.0	955.4	27.6	1200.1	81.2	69	28,983	2,996	246,131	10,558	74	24,599	0.33
B'kyzm	59–70	93.7	178.5	1507.5	37.7	1817.3	53.7	129	37,243	4,280	331,251	12,630	82	22,157	0.19
BCkyz	70–105	89.7	282.0	2153.0	56.4	2334.7	37.3	158	68,200	7,626	261,557	18,145	113	32,774	0.12
Ckyzg	105–150	124.2	356.0	2895.0	79.6	3322.6	45.2	187	70,386	10,802	152,708	21,684	162	109,002	0.14

Sabkha site 4															
Salt crust		222.6	447	4,371	97.0	5393.3	29.3	239	68,910	10,903	159,374	23,119	196	117,432	1.32
Az	0–7	123.0	171	4,545	49.2	4972.4	69.1	375	32,093	5,308	205,284	33,941	82	50,490	0.95
Bkyz	7–20	121.8	157	1,198	28.0	1463.0	72.7	101	33,740	5,807	208,800	30,564	100	22,631	0.28
Bkyzm	20–23	126.2	157	1,072	36.0	1334.6	76.3	90	34,360	6,590	227,854	28,953	76	34,249	2.83
B'kyz1	23–60	132.3	191	1,389	45.8	1725.5	77.9	109	38,587	7,600	263,596	21,245	82	43,602	1.48
B'kyz2	60–90	135.2	263	2,032	55.6	2417.4	60.4	144	59,277	10,288	144,541	21,036	164	128,800	0.10
B'kyz3	90–115	108.3	241	2,056	51.8	2391.5	39.7	156	45,156	7,956	489,204	47,209	125	91,522	0.17
BCkyz	115–123	104.6	249	2,167	54.0	2542.3	37.2	163	26,765	4,832	181,216	37,736	79	57,385	0.18
Cyzg	123–150	111.0	270	2,162	59.6	2540.6	37.3	157	30,387	5,059	152,839	73,866	115	29,573	0.21
Sabkha site 5															
Akyz1	0–10	240.6	808	4,342	159.0	6030.0	83.7	190	61,186	10,421	165,026	20,779	152	99,918	2.33
Bkyz	10–27	145.6	369	1,793	68.4	2485.5	108.6	112	79,243	12,557	213,787	32,645	173	16,381	3.99
Bz	27–35	153.6	416	3,076	97.8	4172.0	119.1	182	25,542	4,638	186,512	29,988	74	46,320	10.21
Bkyz1	35–50	128.6	303	2,643	71.8	3448.0	112.1	180	33,766	5,667	211,478	31,892	101	23,129	8.79
Bkyz2	50–70	121.2	277	2341.5	60.2	3003.6	120.2	166	32,414	6,174	224,128	27,915	76	34,173	5.12
2Bk1z1	70–95	104.2	340	2,824	14.8	3696.9	96.7	189	38,781	7,470	262,301	21,777	83	43,856	0.28
2Bk2z2	95–110	120.8	279	2,355	59.6	3016.4	132.6	167	17,089	2,676	308,656	9,089	43	32,864	0.68
Sabkha site 6															
Akz	0–5	152.6	598.0	4621.0	96.8	6085.8	106.0	239	51,115	9,666	143,060	20,322	157	121,752	4.20
Bz	5–40	129.7	144.5	1684.5	24.6	1886.5	143.4	144	24,786	4,624	166,060	35,720	74	53,986	11.82
Bkyz	40–50	103.0	91.5	1220.5	19.1	1341.4	122.8	124	30,419	5,085	155,998	71,344	118	30,493	8.34
Byzm	50–55	117.8	194.0	2634.0	35.6	3082.6	130.9		23,415	2,241	239,798	11,442	73	19,981	16.18
Ck1z1	55–100	68.1	167.5	2232.5	29.4	2573.8	77.1	206	135,389	17,266	231,816	11,736	254	21,381	0.18
Ck2z2	100–140	60.5	161.0	1904.0	27.8	2187.2	70.8	181	144,362	18,687	193,455	12,268	237	25,094	0.08

Table 8.4 Selected mineralogical properties of the soils

Horizon	Depth (cm)	Gypsum + anhydrite (acetone)[a] (%)	Gypsum, 70°C/90°C (oven wt)[a] (%)	Anhydrite (by difference with oven wt) (%)	Gypsum (thermal) (%)	Anhydrite (by difference with thermal wt) (%)	XRD of the < 2-mm[b] (Relative quantities)	Mineral composition of fine (0.1–0.25 mm) or very fine sand (0.05–0.10 mm) fraction[b] (% of the fraction)
Sabkha site 1								
Cz1	0–3	18.6	17.9	1	–	–	–	
Cz2	3–7	23.6	22.5	1	–	–	–	CB49 CA32 FK7 QZ7 AR1 CD1 FP1 OP1
Cz3	7–16	0.2	1.1	−1	–	–	CA2 HA1 GY1	
Cz4	16–42	0.0	1.1	−1	–	–	–	CB42 CA26 QZ20 FK8 CD2 FP1 PR1
R	42–46	0.0	0.7	−1	–	–	–	
Sabkha site 2					–	–	–	
Salt crust		9.4	9.7	0	–	–	–	
Az1	0–10	13.1	13.8	−1	–	–	–	CB57 QZ15 CA13 FK12 CD2 AR1 FF1
Az2	10–20	4.2	6.9	−3	–	–	–	
Bkz1	20–42	0.0	2.2	−2	–	–	–	CB90 CA5 QZ4 FK2
Bkz2	42–68	0.0	1.6	−2	–	–	AR2 HA1 QZ1 CA1 GY1	
Bkzm	68–92	4.1	5.1	−1	–	–	–	CB79 QZ16 CA7 FK5 CD1
Byz	92–107	0.1	1.9	−2	–	–	–	
Cyzg	107–150	0.0	1.6	−2	–	–	–	

Sabkha site 3					–	–	–	
Salt crust		6.6	5.8	−1	–	–	–	
Az	0–8	8.0	7.2	−2	–	–	–	CB50 CA26 QZ14 FK4 CD2 AR1 FP1 GN1 HN1
Bkyz	8–22	0.1	2.3	−2	–	–	AR3 HA2 CA1	
Bkyz	22–38	0.0	1.3	−1	–	–	–	CB99 CA1 QZtr
Bkyzm	38–56	2.0	3.5	−2	–	–	–	
B'kyz	56–59	0.5	2.4	−2	–	–	–	CB98 CA1 QZ1
B'kyzm	59–70	0.1	1.8	−2	–	–	–	
BCkyz	70–105	0.1	1.7	−2	–	–	–	CB77 QZ13 CA5 FK4 CD2
Ckyzg	105–150	0.1	1.9	−2	–	–	–	
Sabkha site 4	–	–			–	–		
Salt crust		6.3	9.1	−3	–	–	GY2 HA2 CA1 AR1 QZ1	
Az	0–7	4.0	7.8	−4	–	–	CA3 HA3 GY2 AY1	
Bkyz	7–20	0.8	1.9	−1	–	–	CA3 QZ3 GY2 HA1	CB48 CA26 FK16 QZ8 CD2 FF1
Bkyzm	20–23	20.1	22.1	−2	–	–	GY2 CA2 QZ1 HA1	
B'kyz1	23–60	5.7	7.2	−1	–	–	HA3 CA2 QZ2 GY1 AR1	CA46 CB33 QZ13 FK6 CD1 FP1
B'kyz2	60–90	0.1	1.9	−2	–	–	CA2 HA2 QZ1 GY1 AR1	CB68 CA20 QZ6 FK3 CD1
B'kyz3	90–115	0.1	2.1	−2	–	–	HA2 AR2 GY1 QZ1 CA1	CB90 CA5 QZ3 CD1 FK1
BCkyz	115–123	0.0	1.7	−2	–	–	HA2 AR2 CA1 QZ1 GY1	

(continued)

Table 8.4 (continued)

Horizon	Depth (cm)	Gypsum + anhydrite (acetone)[a]	Gypsum, 70°C/90°C (oven wt)[a]	Anhydrite (by difference with oven wt)	Gypsum (thermal)	Anhydrite (by difference with thermal wt)	XRD of the < 2-mm[b] (Relative quantities)	Mineral composition of fine (0.1–0.25 mm) or very fine sand (0.05–0.10 mm) fraction[b] (% of the fraction)
				(%)				
Cyzg	123–150	0.0	2.6	−3	–	–	–	
Sabkha site 5								
Akyz1	0–10	13.0 (±0.0)	12.7 (±1.1)	0	5.8	7	HA3 AY2 CA1 GY1 FK1	
Bkyz	10–27	23.6 (±0.0)	31.1 (±5.1)	−7	7.9	16	HA3 AY2 GY2 CA1 QZ1 FK1	CB52 CA22 QZ13 FK11 FF1
Bz	27–35	41.0 (±0.0)	5.1 (±0.5)	36	2.0	39	AY3 HA2 CA1	CB46 AY21 CA18 QZ13 FK2
Bkyz1	35–50	42.6 (±3.6)	65.1 (±7.4)	−23	11.5	31	CA3 AY1 HA1 GY1 AR1 QZ1	CB64 CA28 FK6 CD1 QZ1
Bkyz2	50–70	28.0 (±0.0)	61.9 (±22.4)	−34	8.0	20	HA2 CA2 GY1 AR1 QZ1	CB71 CA20 FK5 QZ4 CD1
2Bk1z1	70–95	0.2 (±0.0)	3.0 (±0.2)	−3	2.3	0	HA3 AR2 QZ2 CA1 GY1	CB84 CA7 QZ4 FK2 CD1 FF1
2Bk2z2	95–110	2.1 (±0.0)	4.4 (±0.1)	−2	3.8	0	AR2 HA2 QZ1 CA1 GY1	
Sabkha site 6								
Akz	0–5	16.5 (±0.0)	4.0 (±1.0)	12	2.6	14	AY3 CA3 HA3 QZ2 GY2 AR1 FK1	CB40 CA34 QZ12 FK9 CD3 AYtr

Bz	5–40	47.0 (±0.0)	3.3 (±0.6)	44	2.0	45	AY3 HA2 CA1 QZ1 GY1	AY48 CB23 QZ10 CA8 FK7 FD3 HN1
Bkyz	40–50	40.0 (±0.0)	52.4 (±4.7)	−12	6.6	33	HA2 AY2 CA2 GY1	CB10 CA24 QZ12 FK9 AY6 GY6 CD1
Byzm	50–55	30.0 (±0.0)	2.5 (±0.1)	27	0.8	29	AY3 HA1 CA1	AY92 CA5 CB1 FK1
Ck1z1	55–100	0.1 (±0.0)	0.7 (±0.0)	−1	0.5	0	CA3 QZ3 HA1 AY1	CB34 CA29 QZ20 FK11 CD2 FP2 FF1
Ck2z2	100–140	0.0 (±0.0)	0.8 (±0.1)	−1	0.5	0	CA3 QZ1 AY1 GY1 HA1 AR1	

AR aragonite, *FK* orthoclase feldspar, *AY* anhydrite, *CD* chalcedony, *FP* plagioclase feldspar, *OP* opaques, *PR* pyroxene, *GN* garnet, *HN* hornblende

[a] Analyses for pedon 5 and 6 were duplicated. Number in parentheses represents the standard deviation

[b] X-ray data represent relative quantities ranging from 1 to 3 based on peak height. *CA* calcite, *CB* carbonate aggregates, *QZ* quartz, *HA* halite, *GY* gypsum

"group" (gypsum + anhydrite) were concentrated in upper horizons (upper 50 cm) of pedons 1–4, ranging from 0 to 24%. Surface salt crust in pedons 2, 3, and 4 had gypsum + anhydrite ranging from 5 to 9%. Gypsum + anhydrite was concentrated in the upper 70 and 55 cm for pedons 5 and 6, ranging from 13 to 47%. Concentrations were <2% below these depths for the latter two pedons.

Analysis for gypsum by weight loss (Artieda et al. 2006) found reasonably close agreement with the acetone method for pedons 1–4 (Table 8.4). This agreement suggests that no anhydrite was present in the first four pedons. Anhydrite was suspected during the field examination in the Bkyz horizon of pedon 3 and in the B'kyz2 (60–90 cm) and B'kyz3 horizons (90–115 cm) of pedon 4. But very minor amounts (≤0.1%) of gypsum + anhydrite were found in these horizons.

The presence of anhydrite (as indicated by the positive difference between the acetone and weight loss methods; i.e., Eq. 8.1) was found in pedons 5 and 6. Anhydrite was determined by this approach to be in the Bz horizon (27–35 cm) of pedon 5 and the Akz, Bz, and Byzm horizons of pedon 6 in amounts ranging from 12 to 44%.

Negative values for calculated anhydrite using Eq. 8.1, ranging from −12 to −34% (Bkyz1 and Bkyz2 of pedon 5 and Bkyz of pedon 6), reflect greater gypsum measured by weight loss than gypsum + anhydrite by the acetone method. Small negative differences were common for other samples as the difference between methods for pedons 1–4 ranged from 1.0 to −3.8%. These similar values were regarded as generally equivalent, representing methodological differences.

Large negative values for anhydrite using the oven weight loss method (Eq. 8.1) suggest a possible interference or methodological problem. To better understand the problem, both the acetone and weight loss procedures were duplicated for pedons 5 and 6. Low standard deviations for the acetone method suggest good reproducibility. Standard deviations of the weight loss method range from 5 to 22%, illustrating that this method has limited reproducibility. Possible interferences in these samples contributing to the excessive weight loss between 70 and 90 °C may be other minerals (hydrated salts) or clay minerals such as smectite (Lebron et al. 2009). These soils have low clay percentages, and analyses show that no aluminosilicate minerals such as smectite were present in the clay fraction to contribute as a source of errors.

A possible positive interference in the weight loss method by hydrated salts is not apparent. The ECsat for these three horizons in question ranged from 104 to 175 dS m^{-1}, very similar to ECsat from other horizons in these two soils where no negative calculated anhydrite values occurred. Also, other horizons with similar ECsat show good agreement between the two methods. For example, horizons Az1 in pedon 2 and Bkyzm in pedon 3 both have ECsat >97 dS m^{-1} and have gypsum + anhydrite by the acetone methods of 20 and 13%. The corresponding values for the weight loss method are 22 and 14%, respectively.

Thermal gravimetric analysis (TGA) (Fig. 8.4) was performed on all horizons from pedons 5 and 6 as a second method to quantify gypsum by weight loss. While positive interferences are possible with the thermal analysis method, overall, gypsum measured by TGA (Table 8.4) was lower than quantities measured by the oven

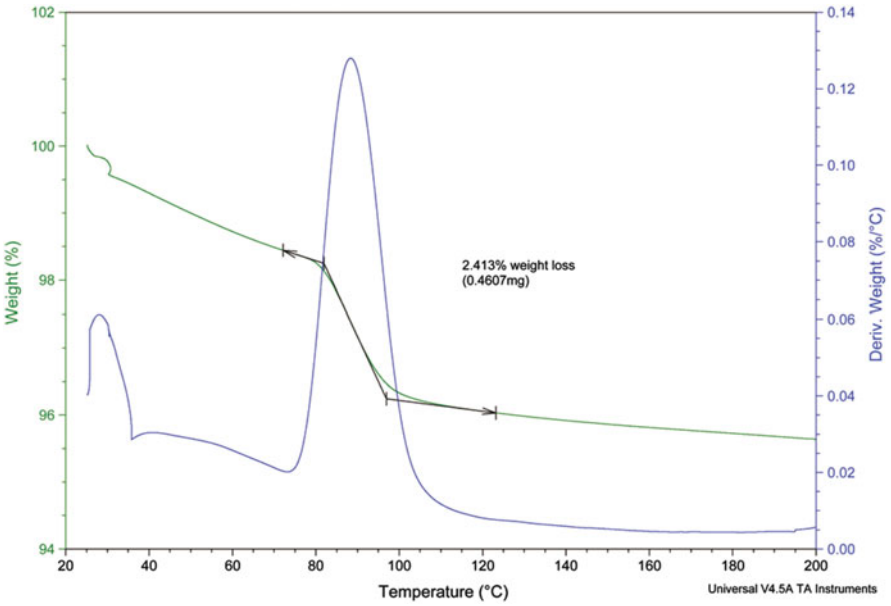

Fig. 8.4 Thermal gravimetric analysis (TGA) pattern illustrating loss of weight from heating the <2-mm soil from the Bkyz1 horizon of pedon 5

method. Good agreement between the two weight loss gypsum methods was achieved with some samples, while large differences in measured gypsum between the two methods also occurred. Large differences in results were those horizons with large negative anhydrite values when using data from the oven method. For example, the Bkyz2 horizon of pedon 5 had 62% gypsum by the oven weight loss method versus 8% gypsum by TGA. Since both methods measure the weight of water loss from gypsum, these TGA data suggest that the oven method has problems for gypsum quantification that are not necessarily interferences of water loss from other minerals.

The TGA results suggest that anhydrite was present in the upper 70 and 55 cm of pedons 5 and 6, respectively, with anhydrite quantities ranging from 7 to 45%. These concentrations are somewhat lower than found in other studies of the sabkha that reported percentages ranging up to 98% (Shahid et al. 2009). The ratio of anhydrite to gypsum in these horizons ranged from 1:1 to 36:1. Largest ratios were present in Bz horizons of both pedons.

8.4.4 X-Ray Diffraction and Optical Analysis

Evaporative minerals in the <2-mm fraction identified by x-ray diffraction (Table 8.4) include calcite, gypsum, halite, aragonite, and anhydrite. No conclusive evidence for bassanite ($CaSO_4 \bullet ½\ H_2O$), mineral that would be considered the intermediary

between gypsum and anhydrite, was found in these samples. Anhydrite was detected by this method in the upper 4 horizons of pedon 5 and all horizons of pedon 6. Detection of this mineral is based primarily on a peak at 0.350 nm, with possible secondary peaks at 0.285, 0.233, and 0.387 nm, and other minor peaks. Relative amounts, based on peak intensity of the 0.35 nm peak, vary. The greatest quantities were in the Bz horizons of pedon 5 and the Akz, Bz, and Byzm horizons of pedon 6. These results are in reasonable good agreement with the anhydrite detected by the TGA method. The only major difference is the Bkyz2 horizon (50–70 cm) of pedon 5, with 20% anhydrite measured by the acetone/TGA method, while no anhydrite was detected in the <2-mm fraction by x-ray diffraction. This may suggest that the acetone/TGA method overestimates anhydrite for some samples, but also the lack of the major 0.350 nm anhydrite XRD peak in the sample does not rule out the presence of the mineral. There were several minor peaks present in the XRD analysis of that horizon that could be assigned to anhydrite.

Anhydrite occurs in a variety of forms and sizes. For example, it forms microcrystalline to coarse crystalline fillings as well as lath- or fiber-like forms (El-Tabakh et al. 2004). Sand-sized anhydrite under the microscope is distinct from other minerals, especially gypsum. It has a refractive index >1.54 and a high birefringence under cross polarized light. Cleavage is generally at right angles or parallel to the mineral axis resulting in elongated, angular mineral forms. Gypsum can be distinguished from anhydrite due to a refractive index <1.54 and low birefringence. Calcite has a variable (double) refractive index (can be both below and above 1.54) depending on direction of orientation, as well as extreme birefringence and rhombohedral cleavage in the macrocrystalline form (Kerr 1977). Often, calcite is microcrystalline in soils and tends to segregate from other minerals (not adsorbed to other mineral surface), forming homogeneous deposits in voids (Chadwick et al. 1987).

Optical analysis (Table 8.4) of the fine and very fine sand fractions shows that carbonate aggregates and calcite were the most common mineral forms identified. Quartz and orthoclase feldspar were also identified in amounts up to 20%. The sand fractions analyzed are derived from the particle size analysis procedure. Washing pretreatments in this procedure will remove all salts and possibly much of the gypsum and anhydrite. Gypsum was found only in the Bkyz horizon of pedon 6, while anhydrite was optically identified in several horizons of pedon 5 and 6, composing 21% in the sand fraction of Bz horizon of pedon 5 and 92% of the sand fraction in the Byzm horizon of pedon 6. The grains of anhydrite are principally elongated and highly birefringent under cross polarized light (Fig. 8.5a, b). These results suggest that gypsum is much more soluble than anhydrite (relative to the PSDA washing procedure).

In thin sections of natural fabric, anhydrite was present as randomly oriented grains in aggregates. This nodular form agrees with both Evans et al. (1969), who identified anhydrite as soft plastic masses that range from having sharp to diffuse boundaries with the surrounding soil matrix, and El-Tabakh et al. (2004), who identified anhydrite beds with this mineral in a nodular form. The largest and most well-developed anhydrite grains were in Byzm horizon of pedon 6. These grains (Fig. 8.6a) ranged up to 0.5 mm in length and were highly birefringent. Figure 8.6b, c

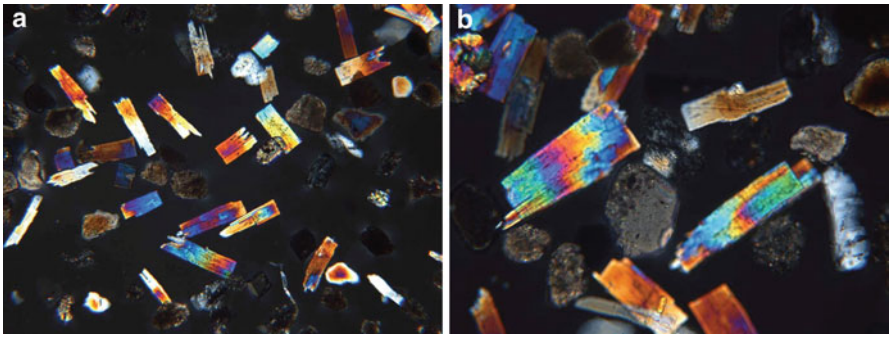

Fig. 8.5 Photomicrograph of anhydrite grains from the very fine sand (0.05–0.1 mm) fraction pedon 6 (Bz horizon). Cross polarized light

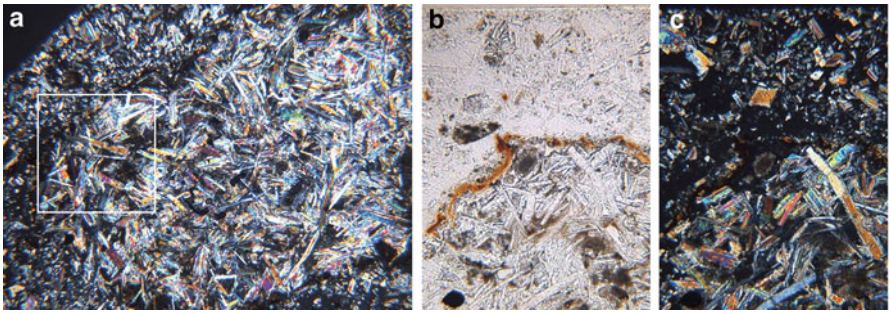

Fig. 8.6 Photomicrograph of the soil fabric of the Bz horizon from pedon 6 illustrating the nodular form of anhydrite aggregates. Anhydrite grains composing this horizon are in the very fine sand size range. Cross polarized light. Photo width = 2.5 mm (**a**). Higher magnification images of the area enclosed by the box in (**a**) both in (**b**) plain and (**c**) cross polarized light. These images illustrate the variety of elongated grains as well as the Fe deposit along the boundary of the nodule. Photo width = 1.1 mm

illustrates frequent occurrence of Fe oxide deposition around the perimeter of the nodules, indicating a hydrologic discontinuity between the nodules of anhydrite and the rest of the soil matrix. The grains in the Bz horizons of pedons 5 and 6 were smaller in size. This is especially true for pedon 5 where anhydrite grains appear to be principally clay and fine silt (Fig. 8.7). These results illustrate that anhydrite occurs in a range of particle sizes in these soils. This difference in the dominant size fraction of anhydrite between horizons suggests a difference in mode of deposition, conditions of formation, or age of the deposit. This difference in size of grains likely accounts for the better agreement between the x-ray diffraction data on the <2-mm fraction and the optical grain count data on a specific sand fraction (Table 8.4) for certain horizons. For example, the Bkyz horizon of pedon 5 has no anhydrite identified in the sand fraction by optical analysis, while anhydrite was present in the x-ray diffraction data for the <2-mm fraction, suggesting anhydrite was present in

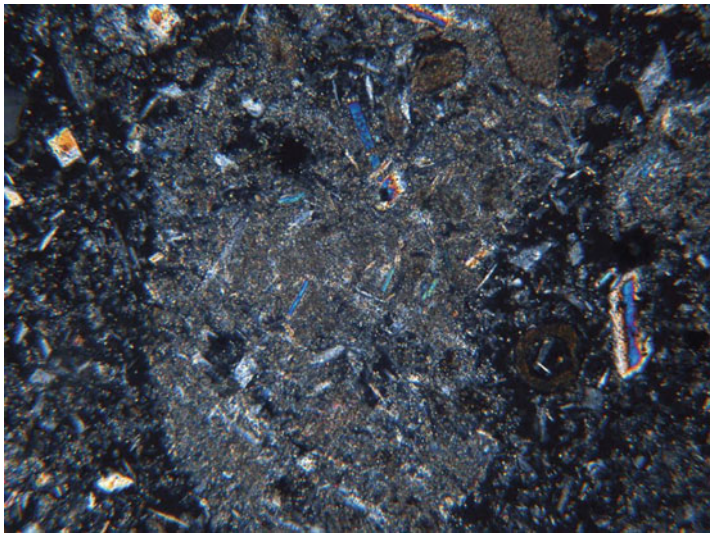

Fig. 8.7 Photomicrograph of the soil fabric of the Bz horizon from pedon 5 illustrating the nodular form of anhydrite aggregates. Much of the anhydrite in this horizon appears to be in the clay and fine silt size range. Cross polarized light. Photo width = 0.53 mm

the smaller particle size fractions only. Also, the Akz horizon of pedon 6 had an XRD anhydrite peak with the relative size of 3, yet had only trace amounts of anhydrite identified in the sand fraction. As mentioned previously, these differences could also be attributed to the dissolution of anhydrite from the sand fraction during PSDA pretreatments used to derive the sand fraction for optical analysis.

8.4.5 Physical Properties

These soils (Table 8.1) are sandy textured, with >75% sand in the <2-mm fraction. Due to pretreatments, the particle size data reflects the loss of soluble salts and much of the gypsum and anhydrite from these samples, but still reflect similar textures as determined in the field. Carbonates and carbonate-coated minerals (e.g., carbonate-coated gypsum) likely remain following pretreatments.

Horizons with large anhydrite concentrations had greater amounts of silt than comparable horizons. For example, the Bz horizon of pedon 5 and the Bz and Bkyz horizons of pedon 6 (all with >30% anhydrite) had silt contents ranging from 52 to 81%. This particle size is generally accompanied by a greater 33 kPa water retention and lower bulk density than other horizons. The bulk density of the three horizons cited above ranged from 0.96 to 1.12 g cm^{-3}, and 33 kPa water retention ranged from 42 to 56%. In contrast, the Byzm horizon in pedon 6 was determined to have 92% anhydrite by optical analysis, but a higher sand content and bulk density than other anhydrite-rich horizon. The difference in this horizon was that it is cemented, unlike the other more friable, anhydrite-rich horizons.

8.5 Discussion

Mineral formation in soils is controlled by the elements present, their concentration and form, as well as chemical and environmental conditions of the pedoenvironment. In the level, coastal region of the Abu Dhabi Emirate, elements in soil solution derived from soluble mineral components of Tertiary deposits underlying the sabkha, as well as from sea and lagoon water intrusion or overland flow, were concentrated via evaporation in the soil vadose zone. The most stable minerals, such as calcium carbonates, were initially deposited. As alkaline anions (principally HCO_3^{-1}) were depleted via calcite deposition, then sulfate minerals, either gypsum or anhydrite, precipitated.

Anhydrite was identified in pedons 5 and 6 by the chemical/weight loss technique, x-ray diffraction, thin section, and optical analysis. The oven method used to measure gypsum and then to calculate anhydrite exhibited poor reproducibility, though appeared to work reasonably well in some samples. Measurement of gypsum by thermal analysis (TGA), followed by anhydrite quantification, did provide more consistent results when compared to other methods (x-ray diffraction, optical analysis). Thermal analysis appears to have promise as a method of choice to quantify gypsum in samples that also contain anhydrite.

X-ray diffraction is an excellent tool to identify the presence of anhydrite in soils, but it only provides qualitative or possibly semiquantitative information. Optical analysis is a reliable method to quantify anhydrite in the particle size range of sand and coarse silt. This mineral has distinct characteristics under the microscope. Anhydrite, unlike gypsum, appears to survive the washing treatment used for particle size analysis, but dry sieving the soil is likely the best option for separating a sample for analysis. The limitation of optical analysis would be that only a limited size range can be easily identified under the microscope (0.02–2 mm) and anhydrite exists in smaller particle size classes as well.

There was no anhydrite detected in pedons 1–4. These four pedons lack the conditions to promote the formation or stability of anhydrite. Pedon 1 is located in the intertidal zone, an area subjected to daily fluctuations of the tide. Pedons 2, 3, and 4 are part of the lower supratidal zone (Shinn 1973), a zone of gypsum formation. Reoccurring seasonal flooding likely limits the formation and stability of anhydrite in these soils.

Pedons 5 and 6, on the highest and most stable part of the sabkha, have anhydrite. This mineral was detected in the upper horizons (0–50 cm) of pedon 5 and all horizons in pedon 6. The Bz horizon of pedon 5 and Bz and Byzm horizons in pedon 6 were the zones of maximum anhydrite concentration in these soils. In Bz horizons, sand, bulk density, and carbonates are at minimum values within the profiles, while silt, water retention, and total S and SO_4 values are at a maximum. While these trends are slightly different for the cemented Byzm horizon, it had the highest total S of all horizons (16.2%). These trends in the data reflect the impact of anhydrite on soil properties. Overall, based on the acetone/TGA method, anhydrite composed 22 and 39% of the mineral matter in the upper 50 cm of pedons 5 and 6, respectively, and about 16% of both pedons between 25 and 100 cm depth,

the mineralogy control section of Soil Taxonomy (Soil Survey Staff 2010). Based on optical analysis data, the weighted average percent of anhydrite in the control section for these two soils are 2 and 17%, respectively.

It appears that anhydrite formation occurs principally by neoformation under extreme conditions of salinity and temperature in these soils. These conditions commonly take place in the capillary zone above the water table, where salts are concentrated by a process referred to as "evaporative pumping" (Hsü and Siegenthaler 1969). Al-Youssef et al. (2006) indicated that necessary conditions for anhydrite formation were Na >0.13 μg L^{-1}, Cl>0.18 μg L^{-1}, total dissolved solids >0.32 μg L^{-1}, and temperatures >25 °C. These concentrations are well below levels of Na and Cl in the saturated paste extracts. Anhydrite appears to initially form nodules that later coalesce into layers or a mosaic of anhydrite. The Bz horizons of pedons 5 and 6 have high amounts of anhydrite and are also the zone of maximum subsurface salinity (91 and 96 dS m^{-1}). In these two Bz horizons, EC1:2 values are nearly double the horizon below and are only exceeded in the pedon by the surface salt concentrations. They are the zones of minimum calcite concentration within the pedons (14 and 4%, respectively), and gypsum is about 5% of the total amount of $CaSO_4$ minerals (anhydrite is 95% of the total). Anhydrite is also present in horizons below and above this zone of maximum concentration, suggesting that anhydrite formation fluctuates somewhat within the profile, likely due to changes of water table depth or temperature. The Byzm horizon in pedon 6 has larger anhydrite crystals than the two Bz horizons. This accounts for the high amount of anhydrite as determined in the sand fraction by optical analysis. It also suggests that this horizon may be the site of older deposits of anhydrite with larger, better-developed crystals.

There is little physical evidence in these soils of alteration of gypsum to anhydrite as suggested by other researchers. Butler (1970) cited that anhydrite is converted from gypsum by either dissolution-precipitation or conversion by dehydration with or without bassanite as an intermediary. He identified solution cavities in gypsum crystals with a rind of coarsely crystalline bassanite and traces of anhydrite. Aref et al. (1997) cited the formation of anhydrite laths enclosing relics of corroded gypsum. El-Tabakh et al. (2004) cited the presence of anhydrite varying between vertically elongated and equidimensional shapes. They regarded the former as an indication of gypsum as a precursor of anhydrite. In this study, some grains of anhydrite in the surface horizons of pedons 5 and 6 were found to have a lenticular appearance similar to gypsum. Figure 8.8a illustrates some grains from the Akyz1 horizon of pedon 5 with the high birefringence characteristic of anhydrite, but with a common shape that is typical of gypsum, such as in the Bkyz horizon of pedon 6 (Fig. 8.8b).

While soil and environmental conditions of this sabkha promote the formation of anhydrite, it is commonly regarded that anhydrite readily converts to gypsum upon exposure and common weathering conditions found in soils (Holliday 1970). Conditions that promote this conversion do not likely exist in this sabkha, as well as other landscapes in the Emirate. Evidence of the stability of anhydrite is present

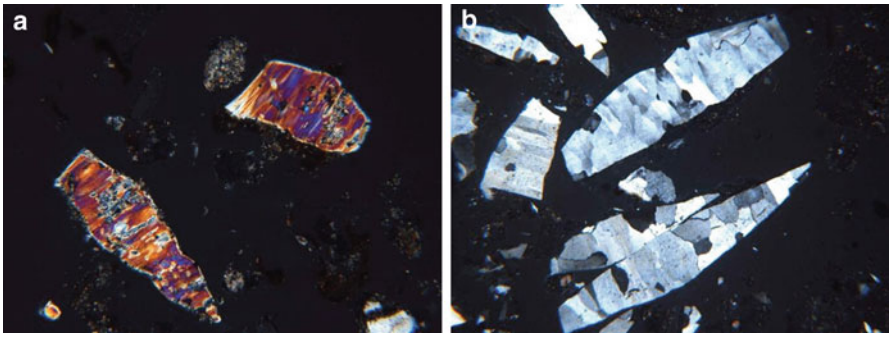

Fig. 8.8 (**a**) Weathered grains of anhydrite from the Akyz1 horizon of pedon 5. Cross polarized light. Photo width = 1.1 mm. (**b**) Gypsum crystal with lenticular morphology similar to Fig. 8.5a from the Bkyz horizon of pedon 6. Cross polarized light. Photo width = 2.5 mm

in anhydrite-rich outcrops scattered throughout the Emirate in upland landscape positions.

Based on regional models of anhydrite formation (Shinn 1973), greater concentrations of anhydrite should be present further inland on the sabkha. Additional evaluation of these landscapes should be conducted to determine the areas of greatest anhydrite content. With further information, the soil maps can be better refined relative to this mineral.

8.6 Conclusion

The formation of anhydrite is a regional phenomenon in hot desert climates of the Middle East, commonly associated with saline coastal areas and a component of carbonate deposition. Six pedons across a sabkha of Abu Dhabi, United Arab Emirates, were sampled for analysis and characterization. Anhydrite was identified and quantified in two of six pedons in this study. Anhydrite quantification by the difference in the acetone dissolution method (gypsum + anhydrite) and weight loss by thermal analysis (gypsum) appears reasonable as a methodology for quantification. This method is in general agreement with other data (XRD, optical grain count of sand) produced in the study. This method will prove useful for the quantification of anhydrite for the purpose of classification of these soils in Soil Taxonomy or other classification systems. Anhydrite quantification was one of the important requirements for inclusion of an anhydritic soil mineralogy family in Soil Taxonomy.

Overall, the presence of anhydrite is documented in the two pedons that are located at the greatest distance from the coast. Zones of maximum anhydrite concentration are occurring in subsurface horizons above the water table, suggesting that the capillary rise and evaporation of groundwater result in the concentration of salts and formation of anhydrite under these environmental conditions.

References

Abdelfattah MA, Shahid SA (2007) A comparative characterization and classification of soils in Abu Dhabi coastal area in relation to arid and semiarid conditions using USDA and FAO soil classification systems. Arid Land Res Manag 21:245–271

Alsharhan AS, Kendall CGSC (2003) Holocene coastal carbonates and evaporates of the southern Arabian Gulf and their ancient analogues. Earth Sci Rev 61:191–243

Al-Youssef M, Stow DAV, West IM (2006) Salt Lake area, Northeastern part of Dukhan Sabkha, Qatar (Chapter 13). In: Khan MA, Boer B, Kurst GS, Barth HJ (eds) Sabkha ecosystems. West and Central Asia, vol II. Springer, Dordrecht, pp 163–181

Aref MAM, Attia OEA, Wali AMA (1997) Facies and depositional environment of the Holocene evaporates in the Ras Shukeir area, Gulf of Suez, Egypt. Sediment Geol 110:123–145

Artieda O, Herrero J, Drohan PJ (2006) Refinement of the differential water loss method for gypsum determination in soils. Soil Sci Soc Am J 70:1932–1935

Burt R (2004) Soil survey laboratory methods manual. SSIR No 42, Ver 4.0. US Government Printing Office, Washington, DC

Butler GP (1970) Holocene gypsum and anhydrite of the Abu Dhabi sabkha, Trucial Coast: an alternative explanation of origin. In: Rau JL, Dellwing LF (eds) Third symposium on salt. Northern Ohio Geological Society, Cleveland, pp 120–152

Chadwick OA, Hendricks DM, Nettleton WD (1987) Silica in duric soils: I. A depositional model. Soil Sci Soc Am J 51:975–982

de Matos JE (1989) The coastal sabkha of Abu Dhabi. Bull 37. Emirates Natural History Group. Available at http://www.enhg.org/bulletin/b37/37_16.htm. Accessed 5 Jan 2010, verified 5 Jan 2010

EAD (2009) Soil survey of Abu Dhabi Emirate. Extensive survey report. Environment Agency, Abu Dhabi, UAE

Elrashidi MA, Hammer D, Seybold CA, Engel RJ, Burt R, Jones P (2007) Application of equivalent gypsum content to estimate potential subsidence of gypsiferous soils. Soil Sci 172(3):209–224

El-Tabakh M, Mory A, Schreiber BC, Yasin R (2004) Anhydrite cements after dolomitization of shallow marine Silurian carbonates of the Gascoyne Platform, Southern Carnarvon Basin, Western Australia. Sediment Geol 164:75–87

Evans G, Schmidt V, Bush P, Nelson H (1969) Stratigraphy and geologic history of the sabkha, Abu Dhabi, Persian Gulf. Sedimentology 12:145–159

Holliday DW (1970) The petrology of secondary gypsum rocks: a review. J Sediment Pet 40(2):734–744

Hsü KJ, Siegenthaler C (1969) Preliminary experiments on hydrodynamic movement induced by evaporation and their bearing on dolomite problem. Sedimentology 12:11–25

Karathanasis AD, Harris WG (1994) Quantitative thermal analysis of soil minerals. In: Amonette JE, Zelazny LW (eds) Quantitative methods in soil mineralogy. SSSA Miscellaneous Publication, Soil Science Society of America, Madison, pp 360–411

Kasprzyk A, Orti F (1998) Paleogeographic and burial controls on anhydrite genesis: the Badenian basin in the Carpathian Foredeep (Southern Poland, Western Ukraine). Sedimentology 45:889–907

Kerr PF (1977) Optical mineralogy, 4th edn. McGraw-Hill, New York

Lambeck K (1996) Shoreline reconstructions for the Persian Gulf since the last glacial maximum. Earth Planet Sci Lett 142:43–57

Lebron I, Herrero J, Robinson DA (2009) Determination of gypsum content in dryland soils exploiting the gypsum-bassanite phase change. Soil Sci Soc Am J 73(2):403–411

Melim LA, Scholle PA (2002) Dolomitization of the capitan formation for reef facies (Permian, West Texas and New Mexico): seepage reflux revisited. Sedimentology 49:1207–1227

NCMS (2009) United Arab Emirates National Center of Meteorology and Seismology. On-line climatic data. Available at: http://www.ncms.ae/english/. Accessed 29 Dec 2009

Sanford WE, Wood WW (2001) Hydrology of the coastal sabkhas of Abu Dhabi, United Arab Emirates. Hydrogeol J 9:358–366

Schoeneberger PJ, Wysocki DA, Benham EC, Broderson WD (eds) (2002) Fieldbook for describing and sampling soils, Ver 2. USDA-NRCS, National Soil Survey Center, Lincoln

Shahid SA, Abdelfattah MA, Wilson MA (2007) A unique anhydrite soil in the coastal sabkha of Abu Dhabi emirate. Soil Surv Horiz 48:75–79

Shahid SA, Abdelfattah MA, El-Saiy AK, Mufti KA (2009) Commercial value assessment of newly discovered anhydrite soil in the coastal lands of Abu Dhabi Emirate. Eur J Sci Res 29(1):36–46

Shinn EA (1973) Sedimentary accretion along the leeward, SE coast of Qatar Peninsula, Persian Gulf. In: Purser BH (ed) The Persian Gulf: Holocene carbonate sedimentation and diagenesis in a shallow epicontinental sea. Springer, Berlin/Heidelberg/New York, pp 199–209

Soil Survey Staff (2010) Keys to soil taxonomy, 11th edn. US Government Printing Office, Washington, DC

Suarez DL (2005) Chemistry of salt-affected soils. In: Tabatabai MA, Sparks DL (eds) Chemical processes in soils. SSSA book series, no 8. Soil Science Society of America, Madison, pp 689–705